

# Infrared spectra at coupled cluster accuracy from neural network representations

Richard Beckmann,<sup>1, a)</sup> Fabien Briec,<sup>1, 2</sup> Christoph Schran,<sup>1, 3, b)</sup> and Dominik Marx<sup>1</sup>

<sup>1)</sup> *Lehrstuhl für Theoretische Chemie, Ruhr-Universität Bochum, 44780 Bochum, Germany*

<sup>2)</sup> *Current Address: Laboratoire Matière en Conditions Extrêmes, Université Paris-Saclay, CEA, DAM, DIF, 91297 Arpajon, France*

<sup>3)</sup> *Current Address: Yusuf Hamied Department of Chemistry, University of Cambridge, Lensfield Road, Cambridge, CB2 1EW, UK*

(Dated: 30 August 2022)

Infrared spectroscopy is key to elucidate molecular structures, monitor reactions and observe conformational changes, while providing information on both structural and dynamical properties. This makes the accurate prediction of infrared spectra based on first-principle theories a highly desirable pursuit. Molecular dynamics simulations have proven to be a particularly powerful approach for this task, albeit requiring the computation of energies, forces and dipole moments for a large number of molecular configurations as a function of time. This explains why highly accurate first principles methods, such as coupled cluster theory, have so far been inapplicable for the prediction of fully anharmonic vibrational spectra of large systems at finite temperatures. Here, we push cutting-edge machine learning techniques forward by using neural network representations of energies, forces and in particular dipoles to predict such infrared spectra fully at “gold standard” coupled cluster accuracy as demonstrated for protonated water clusters as large as the protonated water hexamer, in its extended Zundel configuration. Furthermore, we show that this methodology can be used beyond the scope of the data considered during the development of the neural network models, allowing for the computation of finite-temperature infrared spectra of large systems inaccessible to explicit coupled cluster calculations. This substantially expands the hitherto existing limits of accuracy, speed and system size for theoretical spectroscopy and opens up a multitude of avenues for the prediction of vibrational spectra and the understanding of complex intra- and intermolecular couplings.

## I. INTRODUCTION

Infrared (IR) spectroscopy is one of the most useful analytical tools in chemistry to identify compounds and understand their properties. This is exemplified in studies on the detection of carbon-rich building blocks in space,<sup>1</sup> the nano-imaging of materials,<sup>2</sup> the observation of dynamical couplings in peptides,<sup>3</sup> or the imaging of the proton transfer mechanism in water<sup>4–6</sup> to name but a few examples. However, the interpretation of the measured IR spectra becomes increasingly complicated when moving to more complex systems. Theoretical IR spectroscopy from molecular dynamics (MD) with classical or quantum nuclei<sup>7</sup> provides a unique route to unravel the details of the observed spectra, but requires the highest accuracy in the description of the electronic structure in order to be predictive. Such accuracy is nowadays in many cases best provided by coupled cluster (CC) theory<sup>8,9</sup> — the current “gold standard” in quantum chemistry. At the same time, the computational cost of CC methods, which remains enormous despite much progress in linear-scaling techniques,<sup>10,11</sup> prevents their routine usage for the simulation of IR spectra — except for small prototypical systems and in the absence of temperature and nuclear quantum effects.

Within the last decade, the rise of machine learning (ML) in chemical physics<sup>12–14</sup> has created the opportunity to represent the potential energy surface (PES), governing the dynamics of a given system, at substantially reduced computational cost. With high-dimensional neural network potentials (NNPs) paving the way,<sup>15–17</sup> a multitude of different techniques has been developed to create highly accurate models of interactions;<sup>18–26</sup> see in particular Ref. 27 for a detailed review with a focus on small molecules and reactions. In recent years, ML approaches have progressed towards the description of properties, such as polarizabilities<sup>28</sup> or dipole moments<sup>29,30</sup> which modulate the IR spectral intensities. This has been first shown for electric dipole moments in Ref. 29 based on environment-dependent charges represented by neural networks. Later work has further improved the accuracy of ML dipole models by a combination of atomic dipole moments and charges,<sup>31,32</sup> or extended the formalism to transition dipoles for the prediction of UV absorption spectra.<sup>33</sup> In recent work, the simultaneous prediction of energies, forces and dipole moments has been realized in approaches like PhysNet<sup>34</sup> and Schnetpack.<sup>35</sup> Very elegantly, the dipole moments can be incorporated into the ML model as the response of the energy model to an external electric field.<sup>36,37</sup> Even explicitly learning tensorial properties like polarizability is not beyond the reach of ML based methods through the introduction of tensorial neural networks or E(3)-equivariant neural networks and have been demon-

<sup>a)</sup> Electronic mail: [richard.beckmann@rub.de](mailto:richard.beckmann@rub.de)

<sup>b)</sup> Electronic mail: [christoph.schran@rub.de](mailto:christoph.schran@rub.de)

strated to yield good results for the protonated water dimer<sup>38</sup> and for bulk liquid water,<sup>39</sup> respectively. These seminal contributions highlight that machine learning is emerging as a promising route for the computation of quasi-exact IR spectra at finite temperatures. Even the prediction of such spectra at “gold standard” quantum chemical accuracy seems within reach today, yet it has not been achieved so far for complex molecular systems. Some of us have recently shown how the PES of complex reactive systems, such as protonated water clusters of increasing size, can be represented at CC accuracy using NNPs.<sup>40,41</sup> These clusters have long been of significant interest due to their unique structural properties,<sup>42–45</sup> their rich dynamics<sup>46–48</sup> and their use as model systems for proton transfer reactions in aqueous solutions.<sup>4</sup> The effect of proton transfer on the IR spectrum in particular has been the subject of extended interest, which has spurred key advances in IR spectroscopy.<sup>49,50</sup> For this generic class of large H-bonded systems we push the neural network approach to the next level by representing also dipole moments at close to converged CC accuracy. In particular, we devise a very accurate neural network representation of the dipole moment surface (NN-DMS) for the same set of protonated water clusters for which we parameterized earlier a NN-PES at essentially converged CC accuracy.<sup>40</sup> These developments enable the predictive calculation of IR spectra at full CC accuracy, i.e. including the PES as well as the DMS, based on molecular dynamics simulations to take into account anharmonicity and finite-temperature effects – either using classical point particles or quantum nuclei via path integrals. We note in passing that a first application of our NN-DMS to most accurately compute the IR spectrum of the bare Zundel cation (a.k.a. the protonated water dimer or  $\text{H}_5\text{O}_2^+$ ) based on quasi-exact quantum dynamics propagation, thus fully including nuclear quantum effects, has recently been published.<sup>51</sup> As exemplified here, using differently sized protonated water clusters up to the extended or solvated Zundel complex (a.k.a. the protonated water hexamer or  $\text{H}_{13}\text{O}_6^+$ ) our approach to accurate NN-DMSs holds great promise for the predictive computation of vibrational spectra in the future toward deciphering the complex intra- and intermolecular couplings within large molecular systems on par with modern experimental spectroscopy.

## II. NEURAL NETWORK REPRESENTATION OF DIPOLE MOMENTS

In order to compute IR spectra one first needs an accurate description of the electric dipole moment. We present here an approach to describe the total electric dipole of molecular systems that is based on the high-dimensional neural network representation initially developed by Behler and Parrinello<sup>15</sup> for the description of potential energy surfaces as nowadays routinely used to develop high-quality machine learning potentials.<sup>16</sup>

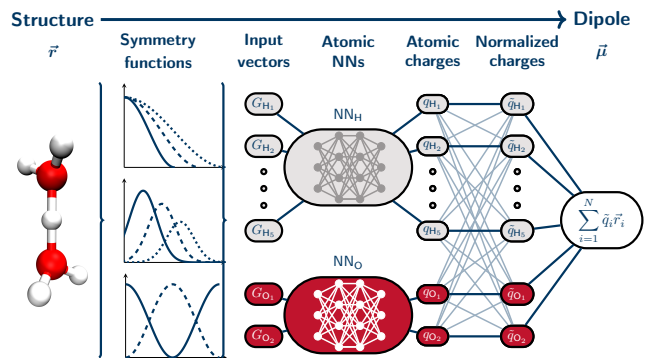


FIG. 1. **Schematic overview of the representation of the total electric dipole moment by high-dimensional neural networks.** In an initial step, the molecular structure is transformed by atom-centered symmetry functions into atomic vectors. Next, this atomic fingerprint is used as input for atomic neural networks that output environment-dependent atomic partial charges. These charges are subsequently normalized in order to conserve the total charge of the system before computing the total electric dipole moment through the standard expression for point charges.

Within the original approach, the total energy of a system composed of  $N$  atoms is computed as a sum over atomic energies  $\epsilon_i$ ,  $E = \sum_{i=1}^N \epsilon_i$ . These atomic energies are the output of associated element-based neural networks that are fully connected feed-forward networks which take as input a set of descriptors of the local atomic environment around the considered atom<sup>15</sup> – we use here the standard atom-centered symmetry functions.<sup>52</sup> It has been demonstrated earlier<sup>29</sup> that this approach can be generalized to the description of the total electric dipole moment  $\vec{\mu}$  of molecular systems. In this case, the electric dipole is computed through the standard expression for a system of  $N$  classical point charges

$$\vec{\mu} = \sum_{i=1}^N q_i \vec{r}_i, \quad (1)$$

where  $q_i$  is the atomic charge associated with atom  $i$  and  $\vec{r}_i$  its position. The output of the element-based neural networks are now these atomic charges which thus depend on the local atomic environment.

This approach, schematically summarized in Fig. 1, has been implemented in RubNet4MD,<sup>77</sup> our software package for training high-dimensional neural networks. The neural network representation of the dipole moment surface (NN-DMS) is trained to reproduce a set of reference dipole moments computed for various representative configurations of the system. The cost function minimized during training is given by the root mean square error (RMSE) of the dipole moment components

$$\mathcal{C} = \frac{1}{3M} \sum_{i=1}^M \sum_{\alpha=1}^3 (\mu_{i,\alpha}^{\text{NN}} - \mu_{i,\alpha}^{\text{ref}})^2 \quad (2)$$

with  $\alpha$  running over the three components of the vector and  $M$  the number of configurations in the training set. Note that this cost function does not impose any constraint on the atomic charges so that the total charge of the system is not fixed. In order to impose the correct total charge  $Q$  of the system, the predicted electric dipole is computed by equation (1) using normalized atomic charges  $\tilde{q}_i$  given by

$$\tilde{q}_i = q_i + \frac{1}{N} \left( Q - \sum_{j=1}^N q_j \right). \quad (3)$$

This particular charge renormalization scheme has been previously suggested and successfully applied in the PhysNet software package.<sup>34</sup> Note that all atomic charges presented in the following are those normalized charges. This approach is different than in previous work<sup>29</sup> where the total charge was included in the cost function thus keeping it only close to the target total charge.

Once an accurate representation of the dipole moment as well as of the potential energy surface is available, high-quality IR spectra can be computed using MD simulations.<sup>7</sup> Indeed, within linear response theory, the infrared (IR) spectrum, described here by the linear IR absorption coefficient per unit length  $\alpha(\omega)$ , can be expressed as

$$\alpha(\omega) = \frac{\pi\beta\omega^2}{3Vc\epsilon_0n(\omega)} \frac{1}{2\pi} \int_{-\infty}^{+\infty} e^{-i\omega t} \langle \vec{\mu}(0) \cdot \vec{\mu}(t) \rangle dt, \quad (4)$$

where  $\vec{\mu}(t)$  is the total electric dipole at time  $t$ ,  $n(\omega)$  the refractive index, which is essentially unity in gas phase,  $\epsilon_0$  the vacuum permittivity,  $V$  the volume (taken to be unity for gas phase),  $c$  the speed of light and  $\beta = 1/k_B T$ . The division by three in the prefactor comes from an isotropic average over the polarization directions of the radiation field. The interested reader is for instance referred to Ref. 7 for more details on theoretical spectroscopy from MD simulations. The IR spectrum is thus directly proportional to the Fourier transform of the time autocorrelation function (ACF) of the total dipole moment,

$$C(t) = \langle \vec{\mu}(0) \cdot \vec{\mu}(t) \rangle. \quad (5)$$

Note that formula (4), where the brackets denote the Boltzmann-weighted statistical (NVT) average at temperature  $T$ , is obtained from the classical limit of the Kubo-transformed formulation of the quantum time ACF.<sup>54</sup> Such ACFs can be directly obtained from MD simulations, thus fully accounting for anharmonicity, mode couplings and finite temperature effects.

### III. COMPUTATIONAL DETAILS

#### A. Neural Network Training

The data set used to train the NN-DMS is composed of the set of configurations generated previously by ac-

tive learning to train the NN-PES.<sup>40,41</sup> For each configuration, the reference electric dipole moments were computed with respect to the origin of the coordinate system using coupled cluster theory including singles, doubles and perturbative triple excitations in the density-fitting approximation DF-CCSD(T), see Refs. 55 for background and methodology. To remove any bias introduced by translations, all configurations were translated so that their center of mass coincides with the origin of the coordinate system. Furthermore, each configuration was rotated at random to remove rotational biases. The augmented correlation-consistent basis set up to double zeta functions<sup>56,57</sup> (aug-cc-pVDZ or AVDZ) is used in combination with the explicitly correlated F12a method<sup>58,59</sup> and an adequate scaling of the triples,<sup>59</sup> thus providing the “DF-CCSD(T\*)-F12a/AVDZ” approach (simply referred to as “CC” in this text). The level of basis set convergence achieved when using that AVDZ basis was confirmed by reevaluating the dipole moments using the computationally much more demanding larger AVTZ basis sets for the approximately 10 000 bare Zundel configurations,  $\text{H}_5\text{O}_2^+$  in our training set as shown in Fig. 2. The direct comparison of the components of all dipole moments at the two basis sets yielded a negligible mean absolute error (MAE) of 0.003 D of AVDZ versus the reference AVTZ dipoles, which is roughly one order of magnitude lower than the usual fitting error obtained with our NN-DMS. In addition, the corresponding error distribution depicted in panel B of Fig 2 reveals that the errors rarely exceed 0.01 D. Overall, inspection of the correlation between AVDZ and AVTZ results shows that calculations with this AVDZ basis set are well converged given the purpose and are, thus, suitable for use as a reliable reference to parameterize the NN-DMS.

All these calculations have been carried out using the Molpro quantum chemistry package.<sup>60,61</sup> Overall, the data set contains 54710 configurations of protonated water clusters ranging from the protonated monomer  $\text{H}_3\text{O}^+$  up to the tetramer  $\text{H}_9\text{O}_5^+$  as well as  $\text{H}_2\text{O}$ . A tenth of these points was chosen at random and removed from the training set to serve as a test set. The remaining points formed the training set to which the NN-DMS was fitted. The NN to predict the dipole moment vectors  $\vec{\mu}$  was constructed with two hidden layers of 30 nodes each using hyperbolic tangents activation functions. An element-decoupled extended Kalman filter algorithm was used to optimize NN weights. Underlying this work is the extension of our in-house RubNNet4MD package for generating high-dimensional neural networks from energies (thus NN-PES) to vectorial properties, namely dipole moments (thus NN-DMS).<sup>77</sup>

#### B. Infrared Spectra

The same procedure has been applied to generate IR spectra of both the bare Zundel cation ( $\text{H}_5\text{O}_2^+$ ) and the much larger extended Zundel complex ( $\text{H}_{13}\text{O}_6^+$ )

as follows: For each system, the canonical ensemble at temperature  $T$  was sampled by a single trajectory with timestep  $\Delta t = 0.25$  fs using a Langevin thermostat<sup>62</sup> with  $\tau = 200$  fs. After equilibration for 10 ps, a phase space snapshot of this trajectory was taken every 500 fs (2000 steps) and used to spawn a non-thermostatted microcanonical (NVE) trajectory, which was then propagated for another 5 ps with the same timestep. Translation of the molecule was removed in post-processing by moving the center of mass to the origin of the coordinate system. While not strictly necessary, this removes the spurious effects close to zero frequency introduced by translational movement of a charged system. The NN-DMS was applied to these centered trajectories to obtain the dipole moment ACF and subsequently the IR spectrum, see equations (5) and (4). For the Zundel cation, 60 trajectories were generated and processed in this manner. At 300 K, the larger  $\text{H}_{13}\text{O}_6^+$  complex can undergo thermal isomerizations into conformations different from that of the extended Zundel cation. To obtain the IR spectrum of only the genuine extended Zundel cation, trajectories exhibiting these rearrangements were not taken into account. Instead, a larger number of NVE trajectories was generated and propagated for 5 ps until 60 trajectories had been obtained which all correspond exclusively to the desired extended Zundel conformation of the protonated water hexamer  $\text{H}_{13}\text{O}_6^+$ .

The Fourier transform of the ACF obtained for each NVE trajectory has been performed by applying a Hann window spanning the entire trajectory to ensure minimal smoothing. The reported IR spectra at temperature  $T$  have been obtained as the average over all 60 individual NVE simulations, spawned from the NVT ensemble as described above. The total dipole moment vectors of the protonated water clusters were autocorrelated every 2 fs in order to provide the required resolution to numerically converge the reported IR spectra up to  $4500\text{ cm}^{-1}$ .

The underlying molecular dynamics simulations with classical nuclei have been carried out using the CP2k software package<sup>63,64</sup> on a previously parameterized and published NN-PES.<sup>40</sup> This NN-PES describes the Born-Oppenheimer energy landscape of protonated water clusters at CCSD(T\*)-F12a/AVTZ accuracy that is largely consistent with the DF-CCSD(T\*)-F12a/AVDZ accuracy achieved here for the dipole moment vector surface of the same protonated water clusters by virtue of the present NN-DMS parameterization, both being close to the complete basis set limit due to using the explicit correlation factor F12a in the reference CC calculations.

#### IV. REACHING COUPLED CLUSTER ACCURACY FOR DIPOLES

We use the high-dimensional neural networks approach to develop a highly accurate NN-DMS for protonated water clusters. This development explicitly includes clusters from the hydronium ion  $\text{H}_3\text{O}^+$  up to the tetramer

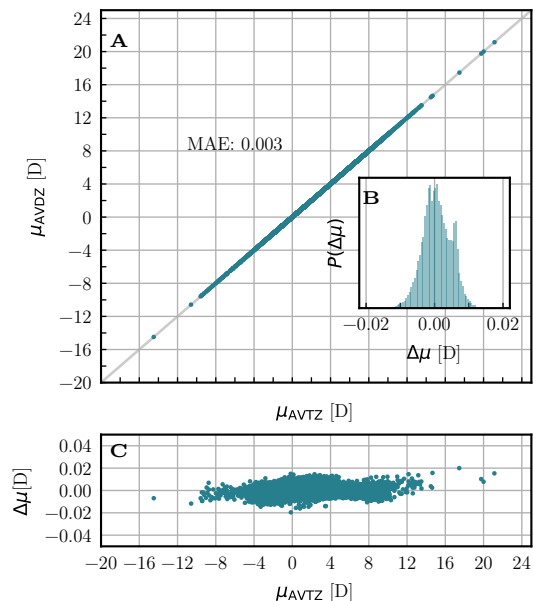


FIG. 2. **Basis set convergence of coupled cluster dipole moments.** A: Correlation between AVDZ and reference AVTZ dipole moment components. B: Distribution of the respective differences  $\Delta\mu$ . C: Differences of AVDZ versus AVTZ dipole moment components plotted against the corresponding AVTZ reference dipole moment components. The dipole moment components  $\mu_\alpha$ ,  $\alpha = x, y, z$ , rather than just its magnitude  $|\vec{\mu}|$  and thus the respective differences  $\Delta\mu_\alpha$  are treated independently in all panels. Dipole calculations for 10 000 configurations of the Zundel cation  $\text{H}_5\text{O}_2^+$  were carried out with the AVDZ and AVTZ basis sets as specified in the text to evaluate the degree of convergence achieved with the AVDZ basis set. The remaining parameters were kept identical between these two sets of calculations and are described in detail in the text.

$\text{H}_9\text{O}_4^+$ , as well as the water molecule. The model is trained against a set of reference dipoles that have been computed using electronic structure calculation at the coupled cluster level including single, double and perturbative triple excitations, CCSD(T), for a large number (54710) of representative configurations of the different clusters. These atomic configurations have been optimally selected previously through an automated fitting procedure used to develop an accurate neural network potential energy surface (NN-PES) for protonated water clusters at the CCSD(T) accuracy level.<sup>40</sup> Additional computational details are provided in section III.

To ascertain the quality of the resulting NN-DMS, a number of stringent tests have been performed. Our final NN-DMS predicts training and test configurations with RMSEs of 0.025 and 0.035 D, respectively. To compare the performance of the model for the differently sized clusters covered by the data set, we disentangle the total RMSE into the various clusters as shown in Fig. 3. It is clear that this NN-DMS accurately describes the dipoles of all clusters up to the tetramer. This analysis reveals that the fitting error increases slightly with clus-



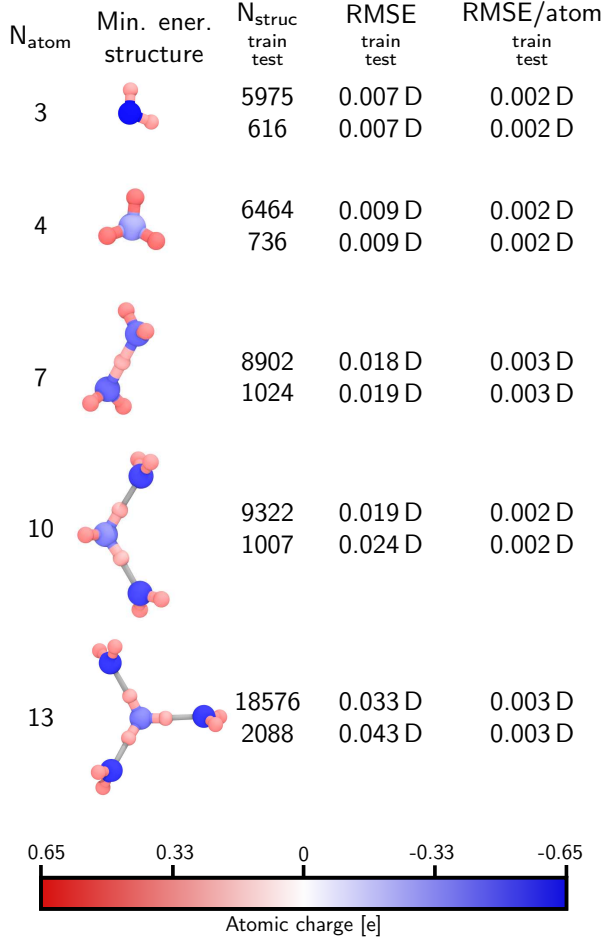


FIG. 3. Overview over all systems used for the parameterization of the NN-DMS for protonated water clusters up to the protonated water tetramer. The color of the atoms in the second column encodes the normalized partial charges  $\tilde{q}_i$  of the atoms within each respective cluster in its global minimum energy configuration as specified by the color scale at the bottom. Note that these partial charges are exclusively fitted to reproduce each cluster's dipole moment without any chosen bias. The third column gives the number of structures in the training and test sets and the fourth one reports the root mean square error for each system in the training and test sets. The fifth column provides the root mean square error divided by the number of atoms in the respective cluster.

ter size. In particular,  $\text{H}_2\text{O}$  and  $\text{H}_3\text{O}^+$  exhibit extremely low RMSE values below 0.01 D for both training and test sets. This does not come as a surprise since the larger number of degrees of freedom make the representation of the reference dipole moment more complex for larger clusters. Nevertheless, we observe a very accurate overall representation of the dipole moments with RMSE values well below 0.05 D. To account for the additional complexity caused by the increased number of degrees of freedom, we also report the error divided by the number of atoms in each cluster in Fig. 3. This reveals a constant RMSE

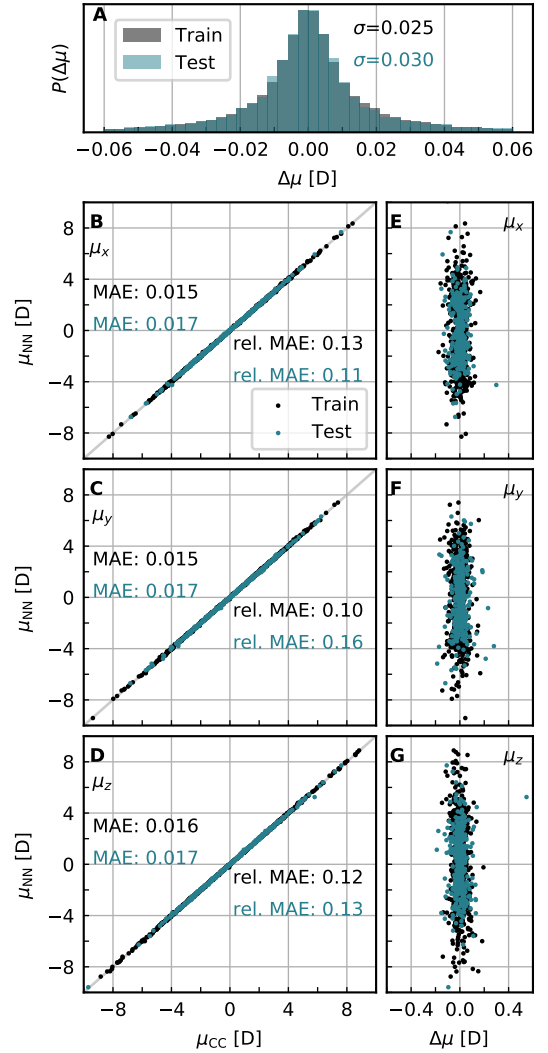


FIG. 4. Validation of the training of the NN-DMS. A: Distribution of errors of the total dipole moment components across training (black) and test (blue) set. B to D: Correlation of total dipoles from the NN-DMS with the reference CC dipoles. E to G: Errors  $\Delta\vec{\mu} = \vec{\mu}^{\text{NN}} - \vec{\mu}^{\text{CC}}$  as a function of the dipole moment values predicted by the NN-DMS. The very few outliers in panels E and G correspond to test set configurations with highly distorted structures which are very high up in potential energy with respect to the relevant PES minima, thus leading to a very low density of training points in such “rate event regions” of configuration space. The total dipole moment components  $\mu_\alpha$ ,  $\alpha = x, y, z$ , rather than just its magnitude  $|\vec{\mu}|$  and thus the respective errors  $\Delta\mu_\alpha$  are treated independently in all panels. Both training and test sets contain all configurations of the protonated clusters from  $\text{H}_3\text{O}^+$  to  $\text{H}_9\text{O}_4^+$  and  $\text{H}_2\text{O}$ .

of 0.002 to 0.003 D per atom for all clusters, indicating that the good performance of the NN-DMS is retained for all clusters. Our errors compare well with Ref. 29 in which a MAE of 0.016 D is reported for methanol over a range of 0.723 D. Here we obtain a total MAE of 0.015 D for five different species over a range of about 16 D and a

MAE of 0.011 D over a range of 8 D for  $\text{H}_5\text{O}_2^+$ , the cluster closest to methanol in terms of size. The obtained accuracy is particularly impressive, given the diverse nature of our data set including not only differently sized clusters, but also various isomers and reactive rearrangement corresponding to proton transfer.<sup>40</sup>

It has previously been shown that the environment dependent atomic charges output by the neural network can capture some aspects of the chemistry underlying a system.<sup>65</sup> We verify this effect here by studying the predicted atomic charges for each cluster in its global minimum energy structure, as represented in Fig. 3 where each atom is colored according to its partial charge as assigned by the NN-DMS. As expected, the predicted charges correlate strongly with chemical intuition: The more electronegative oxygens are always associated with a negative atomic charge while the hydrogens are then assigned a positive charge. Moreover, for the trimer and tetramer, the central oxygen is considerably less negative than the outer oxygen atoms, as expected for a hydronium-like core with three hydrogen atoms. It should be kept in mind that such atomic charges, although resembling other charge partitioning schemes, remain parameters of the model and are not uniquely determined. Nevertheless, they can prove useful for qualitative analysis of related properties, such as the electrostatic potential as shown previously.<sup>65</sup> Finally, we analyze the performance of the model in more detail by looking at the correlation of the predicted dipole components with the reference ones as shown in Fig. 4. Panel A of this figure shows a histogram of the prediction errors, in which each component  $\mu_\alpha$ ,  $\alpha = x, y, z$  of the total dipole moment  $\vec{\mu}$  was treated as an independent prediction, i.e. each configuration contributes three entries to this (and the related) histograms. Histogram A is a simple yet useful first indicator to support the overall quality of the model. The distributions of both, training and test data are very narrow with a standard deviation of 0.025 D and 0.03 D, respectively. With the histogram tails trailing off already around 0.04 D, the overwhelming majority of points have very small errors and even the worst predictions are still satisfactory. The bottom three rows of Fig. 4 show a point-by-point comparison between CC and NN dipoles separated into  $x$ -,  $y$ - and  $z$ -component of the total dipole moments. On the left, the CC dipole component is plotted against the NN dipole component, whereas the right-hand panels show the NN dipole component against the error,  $\Delta\mu_\alpha = \mu_\alpha^{\text{CC}} - \mu_\alpha^{\text{NN}}$ , thus providing a detailed view on outliers and potential systematic errors. Overall, essentially perfect correlation between the prediction and the reference is observed. More importantly there is almost complete absence of outliers or satellite groups. This corroborates that the NN-DMS is providing convincing accuracy for all considered clusters. This analysis does not reveal any differences between the three spatial dimensions, as required for a rotationally invariant representation. Furthermore, it can be seen that test points are represented at essentially the same accuracy as the

training points. Overall, all these tests paint the picture of a highly accurate NN representation of the full dipole moment surface of the five different molecular species for any given configuration considered in the data set.

## V. VALIDATION ON DIPOLE TIME EVOLUTION AND IR SPECTRA

So far, the analysis of the performance of the NN-DMS has concentrated on the fitting accuracy compared to the reference method. In order to put the methodology to a much more stringent test, we focus here on the ability of our dipole moment surface to reproduce dipole fluctuations and real-time dynamics as generated in the course of realistic molecular dynamics simulations. This is a tough challenge to the NN-DMS since the typically subtle time-dependent changes of the dipole moment during molecular vibrations is what gives rise to the IR response. Hence, even tiny errors can have a large impact on the accuracy of the computed IR spectra.

We carried out the required benchmarking for the smallest protonated water cluster featuring a shared proton, for which the very demanding CCSD(T) reference dipoles can still be obtained for the required large number of configurations of about 300 000 in total. To do so, we computed the dipoles of the bare Zundel cation,  $\text{H}_5\text{O}_2^+$ , using both the CC reference method and the NN-DMS over the whole length of the molecular dynamics trajectories; recall that 60 independent trajectories have been computed to rigorously converge the IR spectrum. This is of course a very expensive test since many CC calculations are required, but it grants access to the computation of the converged ACF and thus the IR spectrum from both, the reference CC method and the NN-DMS allowing us to perform a one-to-one comparison. The results are displayed in Fig. 5, where panels A to C show a tiny yet representative excerpt from a random single trajectory out of 60 in total used to compute the IR spectra, separated into the  $x$ -,  $y$ - and  $z$ -components of the total dipole moment  $\vec{\mu}$ . It can be seen clearly that the physical fluctuations caused by configurational changes exceed by far any errors introduced by the NN-DMS. Moreover, the histograms in panels D to F quantify the errors based on all trajectories proving that the NN-DMS retains its excellent performance also in the course of the extensive molecular dynamics simulations.

To compute the IR spectrum from these accurate dipole moments, the ACF of the total dipole moment needs to be computed. Panel G of Fig. 5 depicts this dipole autocorrelation function as computed using the NN-DMS in direct comparison to the reference CCSD(T) dipoles. It can be seen that the ACF retains the same quality already observed in the dipole moment trajectories. Finally, as an end-to-end validation, we have computed the IR spectrum of  $\text{H}_5\text{O}_2^+$  from the dipole ACF in an effort to directly compare the NN-DMS performance to explicit CCSD(T) calculations for a most sensitive ob-

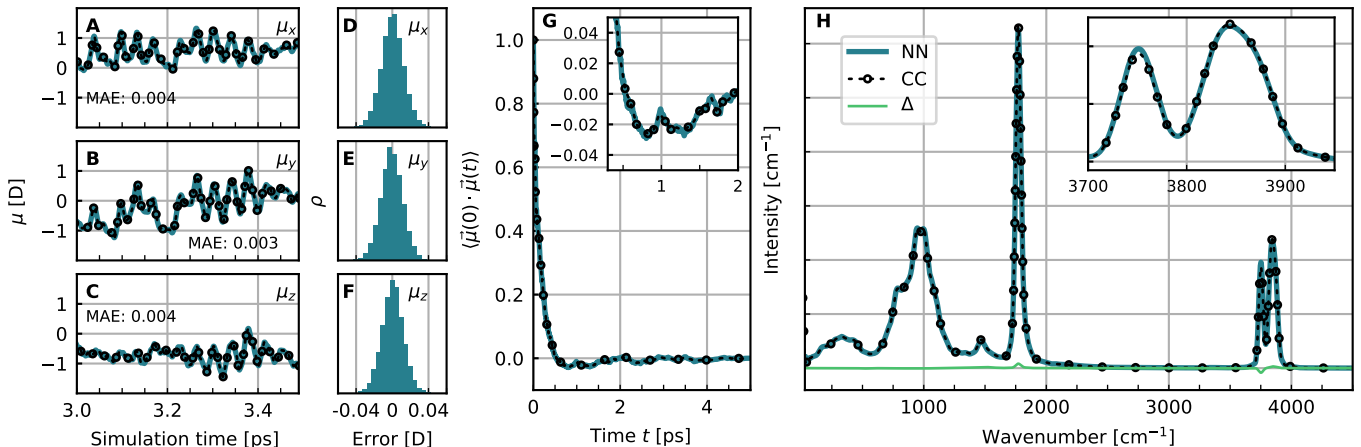


FIG. 5. **Performance of the NN-DMS for the bare Zundel complex,  $\text{H}_5\text{O}_2^+$ .** A to C: Short excerpts from MD trajectories at 100 K comparing the dipole moments from explicit CCSD(T) calculations to those from the NN-DMS separated into their  $x$ -,  $y$ - and  $z$ -components; the corresponding MAE is provided in the respective panels. D to F: Corresponding error distributions over all 60 NVE trajectories generated to compute the IR spectrum in panel H. G: Dipole autocorrelation function from NN and CC dipole moments. H: IR spectrum of the protonated water dimer at 100 K computed from NN and CC dipole moments from the same set of trajectories. The magnified peak in the inset visualizes some very small difference in peak intensity whereas the  $\Delta$  line quantifies the spectral differences as a function of frequency.

servable that is experimentally accessible. Comparing the spectra shown in panel H of Fig. 5 reveals almost perfect agreement between CC and NN spectra. Only two regions of the spectrum show small deviations, one of which is the wavenumber range between 3700 and 3800  $\text{cm}^{-1}$ , which needs to be magnified (see inset in H) to visualize them. The other region exhibiting similar errors is the peak at about 1850  $\text{cm}^{-1}$ . In both cases, however, the error is negligible on the intensity scale of the spectrum, whereas no effects on the peak positions and their shape can be detected. This final test demonstrates that the NN-DMS indeed allows one to rigorously compute IR spectra at essentially converged CC accuracy.

Finally, we stress that the aim of computing the IR spectrum of  $\text{H}_5\text{O}_2^+$  as depicted in panel H of Fig. 5 was to exclusively test the NN-DMS while using classical MD trajectories at 100 K to generate the necessary trajectories (since that computationally economic approach allowed us to explicitly re-compute the dipole moments directly using the CCSD(T) reference method for the same set of sampled configurations). To this end, we employ our recently published highly accurate NN-PES to describe protonated water clusters,<sup>40</sup> with an RMSE of 0.06 kJ/mol per atom while spanning an energy range of several 100 kJ/mol. We refer the interested reader to the original publication for detailed benchmarks of proton transfer paths and MD sampling using this NN-PES, and in particular to Figure 7 therein where we thoroughly demonstrated the accuracy of this NN-PES by comparing to coupled cluster single-point energies that have been computed explicitly along representative trajectory segments generated at several temperatures. Clearly, classical MD simulations are unable to correctly describe the structural dynamics of  $\text{H}_5\text{O}_2^+$  owing to the extremely

complex quantum dynamics of the Zundel cation.<sup>66</sup> Here, we refer to most recent progress<sup>51</sup> on accurate quantum dynamics and IR spectroscopy of  $\text{H}_5\text{O}_2^+$  that results from using the present NN-DMS for protonated water clusters in conjunction with the existing NN-PES<sup>40</sup> both a essentially converged coupled cluster accuracy.

## VI. PREDICTION OF IR SPECTRA OF LARGER CLUSTERS

After the assessment of the quality of the NN-DMS for clusters within the training data, we finally push the model to the limit and test our model for species not considered in the training process – thus probing transferability by entering the extrapolation regime of the dipole network. It has previously been shown that the NN-PES trained on these clusters up to the protonated tetramer retained its predictive power also for larger clusters such as the protonated water hexamer, despite not being part of the training data.<sup>41</sup> This can be attributed to the similarity of the larger clusters to the chemical space spanned by the training set. In the following we will show that this transferability to more complex situations is also achieved by the NN-based dipole surface by performing explicit calculations for the protonated water hexamer in its extended Zundel cation conformation. These advanced simulations reveal that our ML approach provides access to observables such as the IR response at essentially converged CC accuracy of highly complex systems hitherto accessible at such level of theory beyond the systems considered during training of the model.

As a matter of fact, converged CCSD(T) calculations of the protonated water hexamer are prohibitively ex-

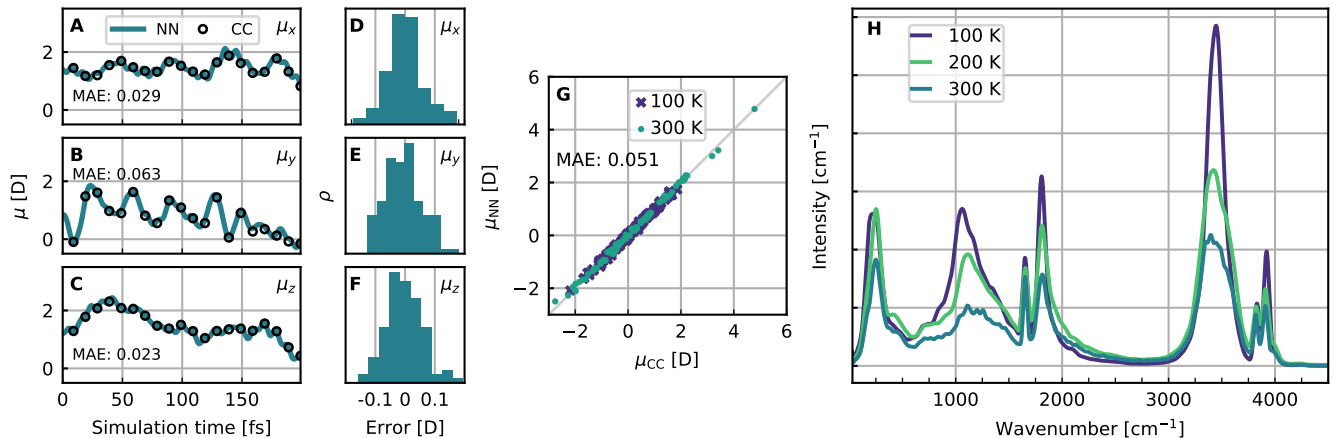


FIG. 6. **Transferability of the NN-DMS for the extended Zundel complex,  $\text{H}_{13}\text{O}_6^+$ .** A to C: Short excerpts from MD trajectories at 100 K comparing the dipole moments from explicit CCSD(T) calculations to those from the NN-DMS separated into their  $x$ -,  $y$ - and  $z$ -components; the corresponding MAE is provided in the respective panels. D to F: Distribution of errors from the short dipole trajectory excerpt (see panels A to C) and 120 additional configurations randomly extracted from MD trajectories at 100 and 300 K (see panel G). G: Correlation of NN dipoles and reference CC dipoles taken from the small MD trajectory excerpt as well as additional configurations randomly extracted from the MD trajectories used to generate the spectra. Associated error distribution are given in panels D to F. H: IR spectrum of the extended Zundel cation at 100 K, 200 K and 300 K, computed from NN dipoles based on 60 NVE trajectories at each temperature.

pensive considering the number of single-point dipole calculations required to statistically converge its finite-temperature IR spectrum, thus preventing us from performing the trajectory-based NN to CC comparison that was still computationally feasible for the protonated water dimer. Instead, we invoke alternative benchmarks as follows. First, we assess the performance of the NN-DMS to describe the real-time dynamics of the dipole moment over 200 fs of a representative MD simulation with respect to the explicit CCSD(T) reference. The evolution of dipole moments along this piece taken from a random trajectory out of 60 used to compute the final IR spectrum at 300 K is shown in panels A to C of Fig. 6, overlaid by explicitly computed CCSD(T) dipole moments every 10 fs. Similar to what was observed for the bare Zundel cation, the NN-DMS prediction agrees very well with the CC reference and, most importantly, captures the subtle but crucial dipole dynamics which fully determines the IR spectrum. Thus, this NN-DMS is transferable to more complex species than those used to learn it.

Secondly, we analyze the long-time stability as to the predictive power of the NN-DMS by quantifying the correlation of NN predictions and the exact CCSD(T) dipole moments as obtained from explicit single-point CC calculations for a realistic validation set build from the extensive MD simulations used to converge the IR spectrum of the extended Zundel complex, namely 120 configurations randomly extracted from all 60 NVE trajectories. The correlation analysis in panel G of Fig. 6 demonstrates that also the large dipole fluctuations as observed only during extensive MD trajectories are well reproduced, thus supporting further the transferability of the NN-

DMS. Although the number of points is relatively small, owing to the tremendous cost of explicit CCSD(T) dipole moment calculations for the extended Zundel complex, it can already be seen from that plot that the NN computations closely match the CC calculations. The detailed error analyses in terms of histograms depicted in panels D to F underlines this assessment by revealing essentially no errors above 0.1 D, being only slightly larger than in the interpolation regime. Despite this expected small decrease in accuracy, the NN-DMS is yielding convincing results across the board as can be seen from the small RMSE of 0.065 D that we obtained within this validation step.

As a final test for the transferability of the NN-DMS, we decided to compute the full IR response of the extended Zundel complex. The simulated IR spectra at 100 K, 200 K and 300 K are shown in panel H of Fig. 6. The most prominent feature of these spectra is the broad signal from about 3300 to 3600  $\text{cm}^{-1}$  which can be ascribed to the red-shifted O-H stretch vibrations of those hydrogen atoms which are involved in intermolecular H-bonds within the complex. These are clearly distinguishable from the high-frequency vibrations of the outermost hydrogen atoms which do not form hydrogen bonds and yield two very sharp signals at 3800 to 4000  $\text{cm}^{-1}$  as is well-known from such largely unperturbed free or dangling OH bonds. At 1600 to 1800  $\text{cm}^{-1}$ , another prominent pair of peaks is visible, corresponding to frequencies known from coupled shared-proton and water bending motion in the bare Zundel complex. At even lower frequencies, a broad yet overall intense signal can be observed between 800 and 1500  $\text{cm}^{-1}$ , which covers the frequency window



where the proton transfer doublet within the bare Zundel complex is located. The spectra at 200 K and 300 K spectrum show the expected thermal broadening with regard to the spectrum at 100 K, but otherwise retains the same features.

It is reassuring to conclude that the finite-temperature IR spectra we computed for  $\text{H}_{13}\text{O}_6^+$  from the highly accurate NN-DMS agrees in its features with the IR response expected for the protonated water hexamer in the extended Zundel conformation. This corroborates that the NN-DMS is able to accurately predict the IR response even for larger systems, not considered during the training of that property surface. This opens up the possibility to systematically push the limits of CC theory to enable the quantitatively predictive computation of physical observables such as anharmonic IR spectra at finite temperatures, otherwise inaccessible by explicit electronic structure calculations.

## VII. CONCLUSIONS AND OUTLOOK

In summary, we have outlined a clear strategy for the prediction of anharmonic finite-temperature IR spectra at coupled cluster accuracy using neural network representations. As demonstrated for differently sized protonated water clusters, learning both, the potential energy and dipole moment surfaces by readily developed machine learning models enables the computation of the converged IR response through exhaustive molecular dynamics simulations. In addition, we have shown that such models can be applied to larger molecular species, not considered in the development of the model, if sufficient care is taken in learning the model and validating its predictions. This makes it possible to systematically push the limits of “gold standard” coupled cluster theory to larger system sizes in order to enable the prediction of physical properties such as IR spectra that are otherwise inaccessible in view of the enormous computational cost of explicit CCSD(T) calculations.

While the IR spectra shown here are based on a classical description of the nuclei, it is known that nuclear quantum effects can have a significant impact on dynamical properties — in particular for high frequency modes. Given that nuclear quantum effects have been accounted for during the development of the training set,<sup>40</sup> we plan to systematically explore as the next logical step approximate quantum dynamics approaches, such as centroid and ring polymer molecular dynamics<sup>67–69</sup> for the prediction of IR spectra using the same machine learning approach. Other avenues to accurately incorporate the quantum dynamics of the nuclei could be quasi-classical approaches<sup>70–72</sup> or multi-configuration time-dependent Hartree (MCTDH) methodologies<sup>73,74</sup> as previously successfully applied to the bare Zundel cation,  $\text{H}_5\text{O}_2^+$ .<sup>66,75</sup> Indeed, our new NN-DMS has been used most recently in conjunction with our NN-PES<sup>40</sup> for protonated water clusters to generate quasi-exact quantum dynamics of the

bare Zundel cation including the corresponding highly accurate IR spectrum<sup>51</sup> in excellent agreement with experiment based on advanced vibrational tree tensor network states (TTNS) techniques,<sup>76</sup> thus going beyond multi-layer MCTDH methods. Given the convincing performance of our NN-DMS with respect to explicit coupled cluster calculations, we think that our machine learning approach holds great promise for the predictive computation of physical observables such as vibrational spectra, notably including the detailed understanding of the intra- and intermolecular couplings within molecular systems of increasing complexity way beyond that of the protonated water dimer.

## DATA AVAILABILITY

The data used to train and validate the NN-DMS presented in this paper together with the final NN-DMS parameterization are available in the Supporting Information to this publication (data-set: All coupled cluster dipole training data of the NNP model sorted by cluster size; benchmarks: All benchmark coupled cluster calculations to compute the spectra of  $\text{H}_5\text{O}_2^+$  and 120 reference dipole moments of  $\text{H}_{13}\text{O}_6^+$ ; example-molpro-input: An exemplary Molpro input file for the computation of the coupled cluster dipole moments; model: All parameters of the NN-DMS) and are also publicly accessible via `nn-dms-supporting-data-v1.0.zip` at <https://doi.org/10.5281/zenodo.6901468>.

## CODE AVAILABILITY

All CC calculations were performed using the Molpro quantum chemistry package.<sup>60,61</sup> The NN-DMS has been constructed using the RubNNet4MD package,<sup>77</sup> while the NN-PES used is available within the Supporting Information of Ref. 40.

## ACKNOWLEDGMENTS

We would like to thank Harald Forbert (Bochum) not only for insightful discussions but for providing us with a program to efficiently and accurately compute IR spectra from MD simulations as well as Hans-Joachim Werner (Stuttgart) for help with the Molpro program package. R.B. acknowledges funding from the *Studienstiftung des deutschen Volkes* and C.S. acknowledges partial financial support from the *Alexander von Humboldt-Stiftung*. Funded by the *Deutsche Forschungsgemeinschaft* (DFG, German Research Foundation) under Germany’s Excellence Strategy – EXC 2033 – 390677874 – RESOLV as well as by the individual DFG grant MA 1547/19 to D.M. This work is supported by the “Center for Solvation Science ZEMOS” funded by the German Federal Ministry of Education and Research and by the Ministry of Culture

and Research of North Rhine-Westphalia. The computational resources were provided by HPC@ZEMOS, HPC-RESOLV, and BoViLab@RUB.

## REFERENCES

- <sup>1</sup>B. A. McGuire, R. A. Loomis, A. M. Burkhardt, K. L. K. Lee, C. N. Shingledecker, S. B. Charnley, I. R. Cooke, M. A. Cordiner, E. Herbst, S. Kalenskii, M. A. Siebert, E. R. Willis, C. Xue, A. J. Remijan, and M. C. McCarthy, *Science* **371**, 1265 (2021).
- <sup>2</sup>F. Huth, M. Schnell, J. Wittborn, N. Ocelic, and R. Hillenbrand, *Nat. Mater.* **10**, 352 (2011).
- <sup>3</sup>C. Kolano, J. Helbing, M. Kozinski, W. Sander, and P. Hamm, *Nature* **444**, 469 (2006).
- <sup>4</sup>C. T. Wolke, J. A. Fournier, L. C. Dzugan, M. R. Fagiani, T. T. Odbadrakh, H. Knorke, K. D. Jordan, A. B. McCoy, K. R. Asmis, and M. A. Johnson, *Science* **354**, 1131 (2016).
- <sup>5</sup>M. Thämer, L. De Marco, K. Ramasesha, A. Mandal, and A. Tokmakoff, *Science* **350**, 78 (2015).
- <sup>6</sup>F. Dahms, B. P. Fingerhut, E. T. J. Nibbering, E. Pines, and T. Elsaesser, *Science* **357**, 491 (2017).
- <sup>7</sup>S. D. Ivanov, A. Witt, and D. Marx, *Phys. Chem. Chem. Phys.* **15**, 10270 (2013).
- <sup>8</sup>R. J. Bartlett and M. Musiał, *Rev. Mod. Phys.* **79**, 291 (2007).
- <sup>9</sup>P. Hobza, *Acc. Chem. Res.* **45**, 663 (2012).
- <sup>10</sup>C. Riplinger, B. Sandhoefer, A. Hansen, and F. Neese, *J. Chem. Phys.* **139**, 134101 (2013).
- <sup>11</sup>D. G. Liakos and F. Neese, *J. Chem. Theory Comput.* **11**, 4054 (2015).
- <sup>12</sup>J. Behler, *J. Chem. Phys.* **145**, 170901 (2016).
- <sup>13</sup>K. T. Butler, D. W. Davies, H. Cartwright, O. Isayev, and A. Walsh, *Nature* **559**, 547 (2018).
- <sup>14</sup>V. L. Deringer, M. A. Caro, and G. Csányi, *Adv. Mater.* **31**, 1902765 (2019).
- <sup>15</sup>J. Behler and M. Parrinello, *Phys. Rev. Lett.* **98**, 146401 (2007).
- <sup>16</sup>J. Behler, *Angew. Chem. Int. Ed.* **56**, 12828 (2017).
- <sup>17</sup>J. Behler, *Chem. Rev.* **121**, 10037 (2021).
- <sup>18</sup>S. A. Ghasemi, A. Hofstetter, S. Saha, and S. Goedecker, *Phys. Rev. B* **92**, 045131 (2015).
- <sup>19</sup>K. T. Schütt, F. Arbabzadah, S. Chmiela, K. R. Müller, and A. Tkatchenko, *Nat. Comm.* **8**, 13890 (2017).
- <sup>20</sup>L. Zhang, J. Han, H. Wang, R. Car, and W. E, *Phys. Rev. Lett.* **120**, 143001 (2018).
- <sup>21</sup>A. P. Bartók, M. C. Payne, R. Kondor, and G. Csányi, *Phys. Rev. Lett.* **104**, 136403 (2010).
- <sup>22</sup>M. Rupp, A. Tkatchenko, K.-R. Müller, and O. A. von Lilienfeld, *Phys. Rev. Lett.* **108**, 058301 (2012).
- <sup>23</sup>A. Thompson, L. Swiler, C. Trott, S. Foiles, and G. Tucker, *J. Comp. Phys.* **285**, 316 (2015).
- <sup>24</sup>A. V. Shapeev, *Multiscale Modeling & Simulation* **14**, 1153 (2016).
- <sup>25</sup>Z. Li, J. R. Kermode, and A. De Vita, *Phys. Rev. Lett.* **114**, 096405 (2015).
- <sup>26</sup>S. Chmiela, A. Tkatchenko, H. E. Sauceda, I. Poltavsky, K. T. Schütt, and K.-R. Müller, *Science Advances* **3** (2017), 10.1126/sciadv.1603015.
- <sup>27</sup>S. Manzhos and T. Carrington, *Chem. Rev.* **121**, 10187 (2021).
- <sup>28</sup>D. M. Wilkins, A. Grisafi, Y. Yang, K. U. Lao, R. A. DiStasio, and M. Ceriotti, *Proc. Natl. Acad. Sci. U.S.A.* **116**, 3401 (2019).
- <sup>29</sup>M. Gastegger, J. Behler, and P. Marquetand, *Chem. Sci.* **8**, 6924 (2017).
- <sup>30</sup>B. G. Peyton, C. Briggs, R. D’Cunha, J. T. Margraf, and T. D. Crawford, *J. Phys. Chem. A* **124**, 4861 (2020).
- <sup>31</sup>M. Veit, D. M. Wilkins, Y. Yang, R. A. DiStasio, and M. Ceriotti, *J. Chem. Phys.* **153**, 024113 (2020).
- <sup>32</sup>A. Grisafi, D. M. Wilkins, G. Csányi, and M. Ceriotti, *Phys. Rev. Lett.* **120**, 036002 (2018).
- <sup>33</sup>J. Westermayr and P. Marquetand, *J. Chem. Phys.* **153**, 154112 (2020).
- <sup>34</sup>O. T. Unke and M. Meuwly, *J. Chem. Theory Comput.* **15**, 3678 (2019).
- <sup>35</sup>K. T. Schütt, P. Kessel, M. Gastegger, K. A. Nicoli, A. Tkatchenko, and K.-R. Müller, *J. Chem. Theory Comput.* **15**, 448 (2019).
- <sup>36</sup>A. S. Christensen, F. A. Faber, and O. A. von Lilienfeld, *J. Chem. Phys.* **150**, 064105 (2019).
- <sup>37</sup>M. Gastegger, K. T. Schütt, and K.-R. Müller, *Chem. Sci.* **12**, 11473 (2021).
- <sup>38</sup>Y. Zhang, S. Ye, J. Zhang, C. Hu, J. Jiang, and B. Jiang, *J. Phys. Chem. B* **124**, 7284 (2020).
- <sup>39</sup>P. Schienbein, *arXiv* (2022), arXiv:2207.08661.
- <sup>40</sup>C. Schran, J. Behler, and D. Marx, *J. Chem. Theory Comput.* **16**, 88 (2020).
- <sup>41</sup>C. Schran, F. Briec, and D. Marx, *J. Chem. Phys.* **154**, 051101 (2021).
- <sup>42</sup>U. Nagashima, H. Shinohara, N. Nishi, and H. Tanaka, *J. Chem. Phys.* **84**, 209 (1986).
- <sup>43</sup>M. Miyazaki, A. Fujii, T. Ebata, and N. Mikami, *Science* **304**, 1134 (2004).
- <sup>44</sup>T. S. Zwier, *Science* **304**, 1119 (2004).
- <sup>45</sup>N. J. Singh, M. Park, S. K. Min, S. B. Suh, and K. S. Kim, *Angew. Chem. Int. Ed.* **45**, 3795 (2006).
- <sup>46</sup>K. R. Asmis, N. L. Pivonka, G. Santambrogio, M. Brümmer, C. Kaposta, D. M. Neumark, and L. Wöste, *Science* **299**, 1375 (2003).
- <sup>47</sup>J. M. Headrick, E. G. Diken, R. S. Walters, N. I. Hammer, R. A. Christie, J. Cui, E. M. Myshakin, M. A. Duncan, M. A. Johnson, and K. D. Jordan, *Science* **308**, 1765 (2005).
- <sup>48</sup>O. Vendrell, F. Gatti, and H.-D. Meyer, *Angew. Chem. Int. Ed.* **46**, 6918 (2007).
- <sup>49</sup>H. A. Schwarz, *J. Chem. Phys.* **67**, 5525 (1977).
- <sup>50</sup>M. Okumura, L. I. Yeh, J. D. Myers, and Y. T. Lee, *J. Chem. Phys.* **85**, 2328 (1986).
- <sup>51</sup>H. R. Larsson, M. Schröder, R. Beckmann, F. Briec, C. Schran, D. Marx, and O. Vendrell, *arXiv* (2022), arXiv:2206.12029.
- <sup>52</sup>J. Behler, *J. Chem. Phys.* **134**, 074106 (2011).
- <sup>53</sup>F. Briec, C. Schran, H. Forbert, and D. Marx, “RubNNNet4MD: The RUB Neural Network for Molecular Dynamics Software Package Version 2,” (2021).
- <sup>54</sup>R. Ramírez, T. López-Ciudad, P. Kumar P, and D. Marx, *J. Chem. Phys.* **121**, 3973 (2004).
- <sup>55</sup>W. Györfy and H.-J. Werner, *J. Chem. Phys.* **148**, 114104 (2018).
- <sup>56</sup>R. A. Kendall, T. H. Dunning, and R. J. Harrison, *J. Chem. Phys.* **96**, 6796 (1992).
- <sup>57</sup>D. E. Woon and T. H. Dunning, *J. Chem. Phys.* **100**, 2975 (1994).
- <sup>58</sup>T. B. Adler, G. Knizia, and H.-J. Werner, *J. Chem. Phys.* **127**, 221106 (2007).
- <sup>59</sup>G. Knizia, T. B. Adler, and H.-J. Werner, *J. Chem. Phys.* **130**, 54104 (2009).
- <sup>60</sup>H.-J. Werner, P. J. Knowles, F. R. Manby, J. A. Black, K. Doll, A. Heßelmann, D. Kats, A. Köhn, T. Korona, D. A. Kreplin, Q. Ma, T. F. Miller, A. Mitrushchenkov, K. A. Peterson, I. Polyak, G. Rauhut, and M. Sibaev, *J. Chem. Phys.* **152**, 144107 (2020).
- <sup>61</sup>H.-J. Werner, P. J. Knowles, G. Knizia, F. R. Manby, M. Schütz, P. Celani, W. Györfy, D. Kats, T. Korona, R. Lindh, A. Mitrushchenkov, G. Rauhut, K. R. Shamasundar, T. B. Adler, R. D. Amos, S. J. Bennie, A. Bernhardsson, A. Berning, D. L. Cooper, M. J. O. Deegan, A. J. Dobbyn, F. Eckert, E. Goll, C. Hampel, A. Hesselmann, G. Hetzer, T. Hrenar, G. Jansen, C. Köppl, S. J. R. Lee, Y. Liu, A. W. Lloyd, Q. Ma, R. A. Mata, A. J. May, S. J. McNicholas, W. Meyer, T. F. Müller III, M. E. Mura, A. Nicklass, D. P. O’Neill, P. Palmieri, D. Peng, K. Pflüger, R. Pitzer, M. Reiher, T. Shiozaki, H. Stoll, A. J. Stone, R. Tarroni, T. Thorsteinsson, M. Wang, and M. Welborn, “MOLPRO, version 2019.1, a package of ab initio programs,”

- (2019).
- <sup>62</sup>G. S. Grest and K. Kremer, *Phys. Rev. A* **33**, 3628 (1986).
- <sup>63</sup>CP2K: Open Source Molecular Dynamics; <https://www.cp2k.org/>.
- <sup>64</sup>J. Hutter, M. Iannuzzi, F. Schiffmann, and J. VandeVondele, *WIRE. Comput. Mol. Sci.* **4**, 15 (2014).
- <sup>65</sup>M. Gastegger and P. Marquetand (Springer, 2020) pp. 233–252.
- <sup>66</sup>O. Vendrell, F. Gatti, and H.-D. Meyer, *Angew. Chem. Int. Ed.* **46**, 6918 (2007).
- <sup>67</sup>I. R. Craig and D. E. Manolopoulos, *J. Chem. Phys.* **121**, 3368 (2004).
- <sup>68</sup>J. Cao and G. Voth, *Journal of Chem. Phys.* **100** (1994), 10.1063/1.467176.
- <sup>69</sup>S. C. Althorpe, *Eur. Phys. J. B* **94**, 155 (2021).
- <sup>70</sup>N. Makri, *Annu. Rev. Phys. Chem.* **50**, 167 (1999).
- <sup>71</sup>J. Beutier, R. Vuilleumier, S. Bonella, and G. Ciccotti, *Mol.Phys.* **113**, 2894 (2015).
- <sup>72</sup>M. Micciarelli, F. Gabas, R. Conte, and M. Ceotto, *J. Chem. Phys.* **150**, 184113 (2019).
- <sup>73</sup>H.-D. Meyer, U. Manthe, and L. Cederbaum, *Chem. Phys. Lett.* **165**, 73 (1990).
- <sup>74</sup>U. Manthe, *J. Chem. Phys.* **105**, 6989 (1996).
- <sup>75</sup>O. Vendrell, F. Gatti, and H.-D. Meyer, *Angew. Chemie Int. Ed.* **48**, 352 (2009).

- <sup>76</sup>H. R. Larsson, *J. Chem. Phys.* **151**, 204102 (2019).
- <sup>77</sup>F. Brieuc, C. Schran, H. Forbert, and D. Marx, “RubNNet4MD: The RUB Neural Network for Molecular Dynamics Software Package Version 2; available upon request at <https://www.theochem.rub.de/go/rubnnnet4md.html>,” (2021).

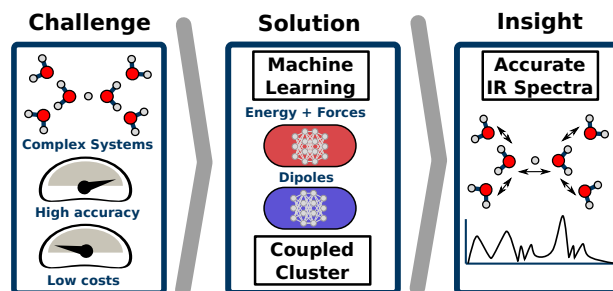


FIG. 7. For Table of Contents Only